Journal of
Materials Chemistry A

Accepted Manuscript

This article can be cited before page numbers have been issued, to do this please use: R. Tang, T. Kaishi, H. Nishihara, T. Ishii, E. Morallon, D. Cazorla-Amorós, T. Asada, N. Kobayashi, Y. Muramatsu and T. Kyotani, *J. Mater. Chem. A*, 2019, DOI: 10.1039/C8TA11005K.

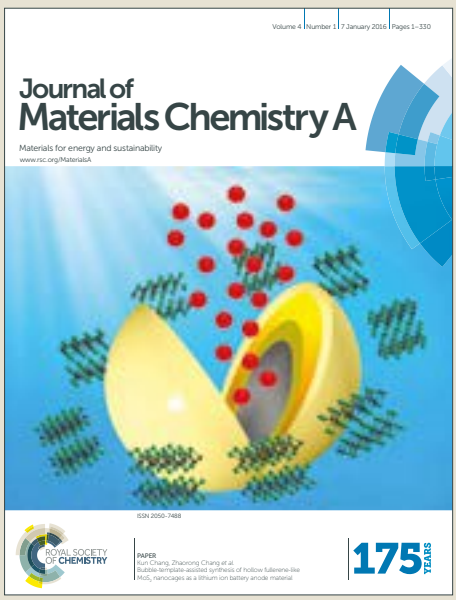

ROYAL SOCIETY OF CHEMISTRY

rsc.li/materials-a

View Article Online
DOI: 10.1039/C8TA11005K

Journal of Materials Chemistry A

PAPER

Insight into the origin of carbon corrosion in positive electrodes of supercapacitors

fiReceived 00th January 20xx,
Accepted 00th January 20xx

DOI: 10.1039/x0xx00000x

www.rsc.org/

Rui Tang,[a] Kaishi Taguchi,[a] Hirotomo Nishihara,*[a] Takafumi Ishii,[b] Emilia Morallón,[c] Diego Cazorla-Amorós,[c] Toshihiro Asada,[d] Naoya Kobayashi,[d] Yasuji Muramatsu[e] and Takashi Kyotani[a]

While activated carbons are used as electrode materials in commercial supercapacitors, they are not stable under high voltage operation especially at a positive-electrode side, and this limits the working voltage of supercapacitors within about 2.8 V in organic electrolyte. Thus, revealing the specific carbon chemical structures causing the corrosion is of great significance to come up with ideas of avoiding the corrosion reactions and eventually to achieve high energy density by expanding the working voltage. In this work, a variety of carbon materials are analyzed with many characterization techniques such as X-ray diffraction, Raman spectroscopy, N_2 adsorption, magnetic susceptibility measurement, and temperature programmed desorption up to 1800 °C, to find out the origin of corrosion reactions in an organic electrolyte. While carbon crystallinity and porosity are not directly related to the positive-electrode corrosion, a good correlation is found between the corrosion charge and the amounts of carbon edge sites terminated by H and oxygen-functional groups which are decomposed and release CO. It is thus concluded that the H-terminated edge sites, phenol, ether and carbonyl groups are electroactive sites for the carbon materials used in the positive electrode of supercapacitor.

Introduction

Electric double layer capacitors, also called supercapacitors, are energy storage devices known for their excellent power performance,[1-11] but their energy density needs further improvement to meet the recent market demands. According to the formula, $E = CV^2/2$, increasing working voltage (V) rather than capacitance (C) is more effective to improve the energy density (E) of supercapacitors. Moreover, the increase of working voltage is important from the practical point of view for reducing the number of cell stacking in a large module to output high voltage (300-500 V) especially for automobile application. It is well known that the stability potential window of an electrolyte medium governs the working voltage of supercapacitors, and thus, propylene carbonate (PC) or acetonitrile is used for commercial supercapacitors from their wider stability potential windows than that of water and relatively low viscosities over a wide temperature range. Nevertheless, it is difficult to increase the working voltage over 2.7–2.8 V, because of the outbreak of many problems such as capacitance drop,[12-15] increase of resistance,[16] and gas evolution.[17-19]

There are two major methods to expand the working voltage of symmetric supercapacitors: (1) the development of stable electrolytes such as ionic liquids[20] and (2) the development of stable carbon materials. The former has been intensively investigated, whereas very stable electrolytes are too expensive for practical applications. On the other hand, the latter has been less studied because it is very difficult to fabricate an appropriate carbon structure that is excellent in every aspect (surface area, electric conductivity, and electrochemical stability). Some limited examples are single-walled carbon nanotubes[21] and graphene mesosponge,[22] both of which endure 4 V as a working voltage in

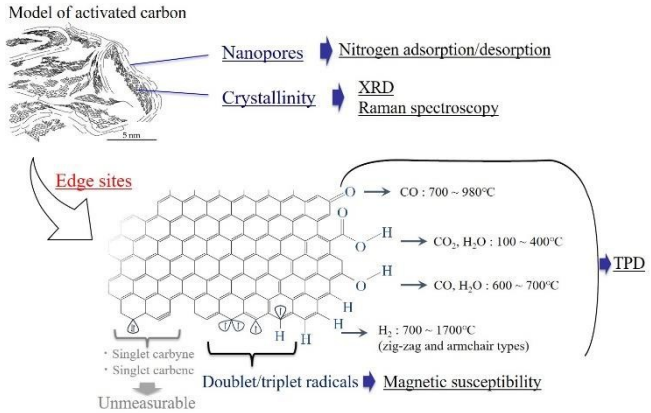

Fig. 1 Illustration of the structure of activated carbon and the techniques used in this work for the characterization of the corresponding specific structures.

[a] Institute of Multidisciplinary Research for Advanced Materials, Tohoku University, 2-1-1 Katahira, Aoba-ku, Sendai, Miyagi, 980-8577, Japan. *E-mail: hirotomo.nishihara.b1@tohoku.ac.jp
[b] International Research and Education Center for Element Science Faculty of Science and Technology, Gunma University, 1-5-1 Tenjincho, Kiryu, Gunma, 376-8515, Japan
[c] Departamento de Química Inorgánica e Instituto Universitario de Materiales, Universidad de Alicante, Apartado 99, 03080, Alicante, Spain
[d] TOC Capacitor Co. Ltd., 3-20-32 Tenryu-cho, Okaya, Nagano, 394-0035, Japan
[e] Graduate School of Engineering, University of Hyogo, 2167 Shosha, Himeji, Hyogo 671-2201, Japan.

† Electronic Supplementary Information (ESI) available. See DOI: 10.1039/x0xx00000x

symmetrical cells even using a conventional organic electrolyte (Et_4NBF_4/PC). The key structural feature in these carbon materials is a very small amount of carbon edge sites which may be the origin of the oxidation reactions when a high voltage is applied. However, like the stable electrolytes, the real application of these carbon materials is also hindered by the high production costs. A more practical solution could be the chemical conversion of such corrosion sites into stable forms in conventional electrode materials (activated carbons). In order to realize this idea, it is first necessary to identify the corrosion sites which would exist in carbon edge sites. However, as shown in Fig. 1, there are a variety of chemical forms in carbon edge sites, and this makes it difficult to clarify the detailed mechanism of carbon corrosion in supercapacitors. Thus, there has been only a limited number of literature which investigated the carbon corrosion in supercapacitors using organic electrolytes which are practically used.

Azaïs *et al.* have reported that the major reason for the capacitance drop and resistance increase is the decomposition of electrolyte on the carbon surface, resulting in the deposition of solid products which block part of porosity, and they have found that surface functionalities affect the deposition.[12] The formation of such solid products has also been reported in PC by Ishimoto *et al*.[23] Moreover, they have concluded that oxygen-functional groups of activated carbon are decomposed by a trace amount of water (contained as impurity) in a lower potential region because CO_2 and CO evolutions were observed by gas chromatography. While these works aimed to reveal "what happens" (generation of solid deposition and gas evolution) upon the supercapacitor corrosion, the relation between carbon structure and supercapacitor degradation has rarely been examined thus far. Cazorla-Amorós *et al.* have reported that the stability of activated carbon electrode is improved by removing most of oxygen functional groups.[24] It is further reported by Yang *et al.* that the presence of many functional groups like carboxyl, lactone and phenol groups led to high gas evolution.[25] These studies suggest that undesirable effects are caused by oxygen-functional groups. However, it is still difficult to understand the comprehensive relationship between carbon structures and supercapacitor degradation, because only limited types of carbon materials have been examined with limited characterization techniques.

In this work, the carbon structural properties and corrosion behaviours of a variety of carbon materials are systematically investigated to identify the common carbon corrosion sites in a positive electrode. Nine kinds of very different carbon materials with a variety of micro/meso/macroporosities are used (Table 1), including three activated carbons, four carbon blacks, reduced graphene oxide (rGO) and zeolite-templated carbon (ZTC).[26] The characterization techniques used in this paper are summarized in Fig. 1. Nanoporous structure of carbon is characterized by nitrogen adsorption/desorption. The crystallinity of carbon is analysed by X-ray diffraction (XRD) and Raman spectroscopy. The properties of edge sites are characterized by two methods. The first method is magnetic susceptibility measurement which can detect triplet carbenes[27] and σ-radicals (doublet) which possibly exist as dangling bonds, and also π-radicals at H-terminated zigzag edge sites.[28] Such radical sites may be highly reactive. In addition to these species, the presence of singlet carbyne and singlet carbene is theoretically predicted,[27] but they cannot be detected by the magnetic susceptibility measurement, and are not considered in this work. The second method is a special temperature programmed desorption (TPD) which allows the detection of all edge sites that are terminated with H or oxygen-functional groups by the quantitative measurement of H_2, H_2O, CO, and CO_2 gas evolutions up to as high a temperature as 1800 °C.[29] Note that conventional TPD is operated up to 1000 °C, which is not high enough to desorb all H atoms from edge sites as H_2. Unlike surface analysis such as X-ray photoelectron spectroscopy (XPS), TPD allows bulk analysis, and is more capable for quantitative measurement. By comparing the aforementioned carbon properties with the electric charges associated with carbon corrosion, we try to seek out the factors affecting electrochemical degradation at a relatively early stage of corrosion process.

Table 1 A list of nine carbon materials used in this work.

Abbreviation	Remarks
AAC	An anthracite-derived activated carbon (3650 $m^2\ g^{-1}$)[30]
AACH2	Prepared by H_2-treatment (850 °C for 1h) of AAC[24]
YP50F	A coconut-shell-derived steam-activated carbon (Kuraray Chemical Co., Ltd.)
BP	Carbon black (BLACK PEALS 2000; Cabot Co., Ltd)
DB	Carbon black (Denka Black; Denka Co., Ltd)
XC72	Carbon black (VULCAN XC72; Cabot Co., Ltd)
KB	Carbon black (Ketjen Black EC-300J; Lion Specialty Chemicals., Ltd)
rGO	Reduced graphene oxide (Aldrich Co., Inc.)
ZTC	Zeolite-template carbon prepared by our group (3598 $m^2\ g^{-1}$)[26]

Results and discussion

Cyclic voltammetry

Fig. 2a shows the CV results on YP50F (an activated carbon used for commercial supercapacitors) when stepwise expanding the upper limit potential from 0.5 V to 1.9 V. In each potential range, the anodic current, which is increased by corrosion reactions, reaches the maximum at the upper limit potential. Previously, we have reported that the first stage of corrosion occurs even at 1.0 V (vs. $Ag/AgClO_4$), involving the oxidation of carbon edge sites by propylene carbonate.[26] Ishimoto *et al.* have reported that oxygen-functional groups of the carbon electrode are decomposed by a trace amount of H_2O to generate CO and CO_2 gases above 1.2 V.[23] Furthermore, propylene carbonate is decomposed and polymerized above 1.65 V.[23] In Fig. 2a, the maximum anodic current gradually increased from 0.5 to 2.1 V, corresponding to the evolution of the prior mentioned corrosion modes. Above 1.7 V, current density decreases, suggesting the decrease of carbon surface area as well as the loss of electric double layer capacitance, because of the polymer deposition.

In this work, we measured the CV patterns of nine kinds of carbon materials with the upper limit potential from 0.5 V to 1.9 V. For each potential range, the irreversible electric charge (Q_{ir}) is calculated by subtracting the total charge during a negative-direction scan above an open circuit potential from the one during a

View Article Online
DOI: 10.1039/C8TA11605K

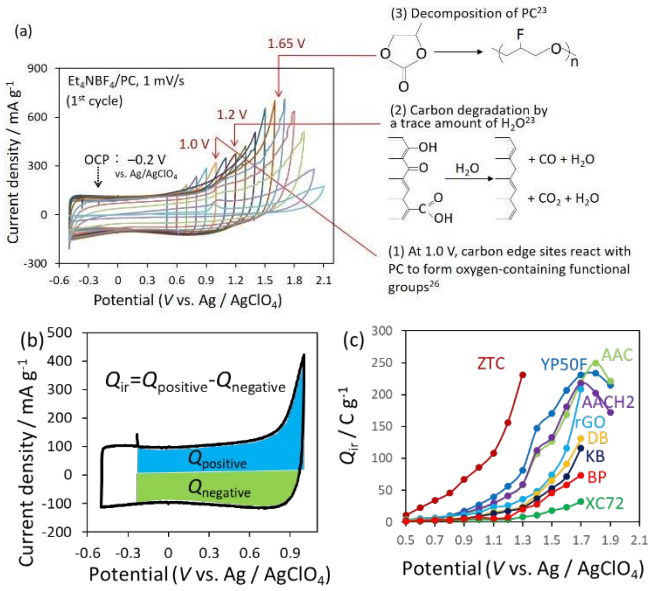

Fig. 2 (a) CV scans at different potential ranges on YP50F. Only the 1st scan results are shown. Insets explain the degradation modes reported in literature. (b) An example of calculating the Q_{ir} of YP50F. (c) The change of Q_{ir} depending on the upper limit potential for nine carbon materials.

positive-direction scan to extract the net corrosion charge associated with electrochemical oxidation apart from the effect of electric double layer capacitance (Fig. 2b). The change of Q_{ir} with the upper limit potential of CV for all the samples is summarized in Fig. 2c. It is found in YP50F that the change of Q_{ir} is in agreement with the change of the maximum anodic current seen in Fig. 2a. In other words, Q_{ir} also reflects the above corrosion modes. Thus, in this work we use Q_{ir} to quantify the positive-electrode degradation of supercapacitor. From the potential at which Q_{ir} rapidly increases as well as the intensity of Q_{ir}, the stability of a carbon sample can be roughly grasped: the onset potential for the Q_{ir} rise becomes higher and Q_{ir} becomes smaller when the carbon sample is more stable. In this work, we focus on the initial carbon degradation occurred at 1.0 V, and use Q_{ir} (unless otherwise noted, Q_{ir} is the value at 1.0 V) as an indicator of corrosion. Among all the carbons, ZTC shows the highest Q_{ir}, while XC72 the lowest. Hereafter, we try to find the factor(s) which dominates the stability of carbon against positive-electrode corrosion.

Nanoporosity

Generally, nanoporosity affects heterogeneous reactions. Pore size, shape, and dimension govern the mass transportation, and surface area correlates with the number of reaction sites. In this work, we use a very small scan speed (1 mV s^{-1}) for CV, and the diffusion-limited process for the corrosion reactions can be avoided, as is shown later. Thus, we focus only on the effect of surface area.

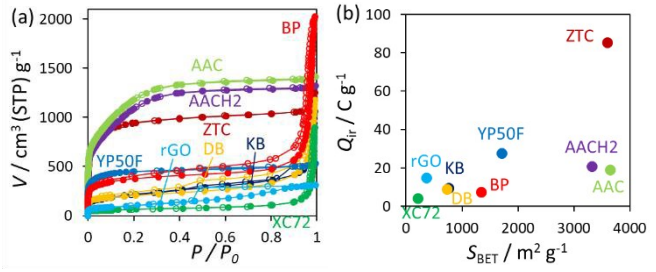

Fig. 3 (a) N_2 adsorption-desorption isotherms of carbon samples. Adsorption and desorption data are shown by solid and blank symbols, respectively. (b) The plot of Q_{ir} against specific surface area (S_{BET}).

Fig. 3a shows nitrogen adsorption-desorption isotherms of the samples. ZTC and YP50F show typical type-I isotherms,[31] and they are microporous materials. AAC shows gradual N_2 uptake at P/P_0 = 0.01–0.3, indicating the presence of relatively small (2–3 nm) mesopores. AACH2 shows only slight decrease of N_2 adsorption amount compared to that of AAC, and it is thus found that the H_2 treatment at 850 °C does not significantly change the nanoporosity, while the surface functional groups are greatly changed. BP, KB, DB and rGO show the feature of a type-IV isotherm with slight hysteresis, indicating the presence of some amount of mesopores. XC72 shows a type-II isotherm, showing its poor micro/mesoporosity. Some carbon blacks show a large uptake above P/P_0 = 0.9, corresponding to the capillary condensation of N_2 in large mesopores/macropores existing at the inter-spaces of carbon nanospheres. The textural properties of the carbon samples are summarized in Supplementary Table S1 and Fig. S1.

Fig. 3b shows Q_{ir} of each carbon, plotted against specific surface area (BET surface area, S_{BET}, is used). Although ZTC (3598 m^2 g^{-1}), AAC (3650 m^2 g^{-1}) and AACH2 (3318 m^2 g^{-1}) have similar specific surface areas, their Q_{ir} values are very much different. Also for the other samples, almost no correlation can be found between Q_{ir} and S_{BET}. Thus, specific surface area is not responsible for the early-stage degradation, and this is consistent with the conclusion reported by Xu *et al.*[32] These results can be ascribed to the non-uniform distribution of reaction sites in carbon materials, because of the intrinsic anisotropy of a graphene sheet which is the minimal structural unit as shown in Fig. 1. Considering that the basal planes should be more stable than the edge planes, it is deduced that carbon corrosion sites exist only at the carbon edge planes.

Crystallinity

Generally, highly crystalline graphite is very stable against corrosion, while low-crystalline activated carbons are not. This is because the amount of edge sites tends to decrease with increasing carbon crystallinity.[22] We thus investigate the effect of crystallinity degree on the electrode corrosion by using XRD and Raman spectroscopy.

Fig. 4a shows the XRD patterns of the carbon samples. The crystallinity degree of non-graphite carbon materials can be roughly estimated from the two broad peaks at around 2θ = 26° and 43°, corresponding to the carbon 002 and 10 peaks, respectively. The 10 peak is derived from the in-plane diffraction of a graphene sheet (instead of 11 peak, 10 peak is used because the 11 peak is too small), while the 002 peak is from the ordered stacking of graphene sheets. The full width at half maximum (FWHM) of an XRD peak, β, has directly to do with the crystallite size (L), through the following Scherrer equation:

$$L = \frac{K\lambda}{\beta cos\theta} \qquad (1)$$

where K, λ, and θ are a shape factor, X-ray wavelength, and the Bragg angle, respectively. Thus, a sharp 10 peak (small β) means a large graphene-domain size (a small amount of edge sites), and vice versa. Accordingly, Q_{ir} may increase along with the FWHM of the

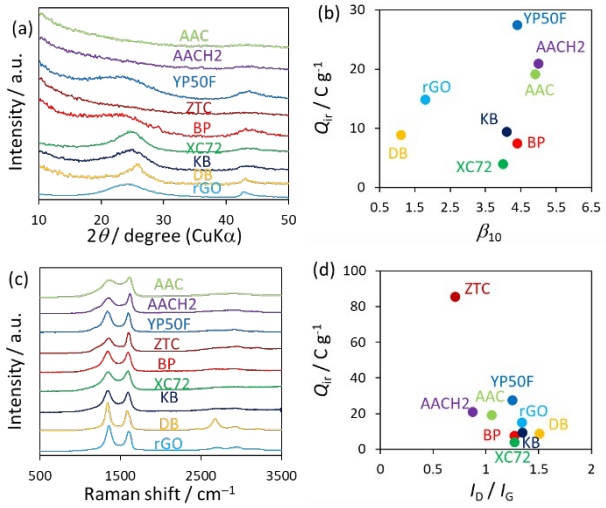

Fig. 4 Influence of crystallinity. (a) XRD patterns. (b) The plot of Q_{ir} against FWHM of the carbon 10 peak (the data of ZTC is not shown as it does not display 10 peak). (c) Raman spectra which are normalized by the intensity of G-band. (d) The plot of Q_{ir} against I_D/I_G.

carbon 10 peak, β_{10}. However, as shown in Fig. 4b, no clear correlation can be seen between Q_{ir} and β_{10}. There are two possible reasons: (1) the carbon 10 peak can reflect only continuously flat domains. When a continuous graphene sheet is curved, β_{10} corresponds only to the flat portion rather than the whole graphene size. Low-crystalline carbons, like activated carbons[33] and ZTC,[34] consist of defective and significantly curved graphene sheets, so that β_{10} does not necessarily correlate with the amount of edge sites. (2) Not all edge sites are responsible for the carbon corrosion. As shown later by the TPD analysis, not only (1) but also (2) is the case, and consequently, XRD cannot predict the tendency of carbon corrosion. Note that the FWHM of the carbon 002 peak, β_{002}, also has not any correlation with Q_{ir} (Supplementary Fig. S2).

Raman spectra of the carbon samples are shown in Fig. 4c. Each spectrum was deconvoluted into four bands including the graphitic band (G band), the disorder band (D band), the band ascribed to amorphous carbon (Am band) and the band ascribed to sp^3-bonded carbon atoms (P band) by using the method reported elsewhere.[35] A typical curve-fitting result of AAC can be found in Supplementary Fig. S3. The intensity ratios of the D band to the G band (I_D/I_G ratios) are calculated. It is generally anticipated that the carbon crystallinity degree can be roughly judged by the I_D/I_G ratio or the FWHM of G band. In Fig. 4d, it is found that there is no correlation between Q_{ir} and I_D/I_G ratios. Note that the FWHM of the G-band has nothing to do with Q_{ir} (Supplementary Fig. S4). The results shown in Figs. 4b, 4d, S1 and S3 demonstrate that the carbon crystalline properties analysed by means of XRD and Raman spectroscopy are not directly related to carbon oxidation in positive electrode. A more direct investigation on the effect of carbon edge sites on the electrochemical degradation is necessary.

Carbon edge sites

The results described above illustrate that the amounts of carbon degradation sites are not correlated with the surface area and crystallinity of carbon materials. Accordingly, gas adsorption, XRD, and Raman spectroscopy are useless to predict the electrochemical stability of carbon materials. The question is how to detect the

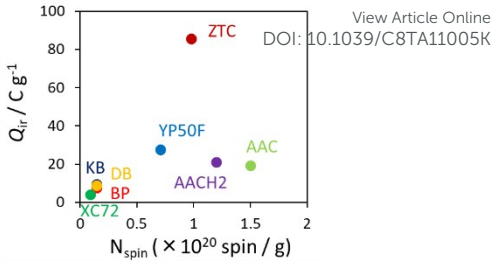

Fig. 5 The plot of Qir against spin density. The total spin quantum number is assumed to be 1/2.

carbon degradation sites which should exist at carbon edge sites, in a variety of structures shown in Fig. 1. To answer this question, we have applied two techniques for the quantitative analyses of different edge sites.

The first method is the magnetic susceptibility measurement which can determine the spin density (N_{spin}) in carbon materials. Spins exist at triplet carbenes,[27] σ-radicals (doublet), and π-radicals[28] (the H-terminated zigzag edge sites). Although the amount of such radical species is relatively small compared with the entire amount of H-terminated edge sites (Supplementary Table S2), the radical sites may be highly reactive and thus it is necessary to examine their effect on electrochemical reactions. However, as Fig. 5 shows, no clear correlation can be found between Q_{ir} and the spin density, indicating that radicals existing in carbon materials are not the origin of the carbon corrosion in positive electrode.

Thus, we applied the advanced TPD technique[29] which can detect the entire edge sites terminated by hydrogen or oxygen-functional groups, by desorbing them as CO, CO_2, H_2O and H_2. Fig. 6 shows the gas evolution patterns (TPD patterns) for all the samples. As is found from Fig. 6a, ZTC, AAC, YP50F, DB and rGO show relatively intense CO evolution, demonstrating the presence of acid anhydrides, ethers, phenols and carbonyl groups in their carbon frameworks.[36] In Fig. 6b, rGO, AAC, and ZTC show a broad peak of CO_2 at the range of 200 °C to 900 °C, and this is ascribed to the decomposition of carboxylic acids, acid anhydrides, and lactones. BP shows a sharp peak at 700 °C, probably corresponding to

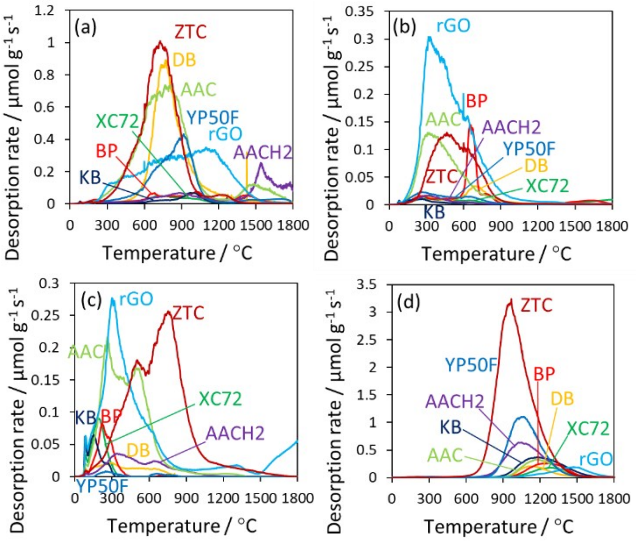

Fig. 6 Evolution of (a) CO, (b) CO_2, (c) H_2O and (d) H_2 during the TPD measurement.

View Article Online DOI: 10.1039/C8TA11005H

lactones.[36] Unlike CO and CO_2 evolutions, the origin of H_2O evolution (Fig. 6c) has not been clearly assigned in literature, and there are several possibilities: (1) dehydration of neighbouring carboxyl groups, (2) dehydration of neighbouring hydroxyl groups and (3) desorption of water adsorbed in carbon pores. The H_2O evolutions of rGO and AAC show some overlapping with the CO_2 evolutions, while H_2O evolution of ZTC overlaps with its CO evolution. Thus, the effect of (1) is significant in rGO and AAC, whereas (2) may be dominant in ZTC. The release of H_2 (Fig. 6d) takes place in the range of about 700 to 1600 °C. ZTC shows the largest release amount of H_2, demonstrating the existence of a large amount of H-terminated edge sites.

From Fig. 6, the effect of H_2 treatment on AAC can be clearly seen. CO, CO_2, and H_2O evolutions are remarkably decreased in AACH2, while H_2 evolution is increased, indicating that most of the oxygen-functional groups were replaced with H-terminated edge sites. Additionally, the porosity is not greatly changed by the H_2 treatment (Fig. 3a). Thus, the effect of different chemical forms of carbon edge sites can be discussed by comparing AAC and AACH2.

Figs. 7a-d show the plot of Q_{ir} against the total evolution amounts of CO, CO_2, H_2O, and H_2, respectively. As mentioned in the introduction, the undesirable effects caused by oxygen-functional groups have been reported in literature,[25] whereas no correlation was found between Q_{ir} and the amounts of CO, CO_2 or H_2O evolutions in the present data (Fig. 7a-c) using a variety of different carbon materials. Indeed, AAC and AACH2 show almost the same Q_{ir} despite their very different amount of oxygen-functional groups. On the other hand, a good correlation can be found between Q_{ir} and H_2 evolution amount (Fig. 7d). This suggests that the irreversible faradic reactions at 1.0 V start mainly at the hydrogen terminated edge sites of carbon materials in supercapacitors using the organic electrolyte (Et_4NBF_4/PC). To the best of our knowledge, no one has found such a good correlation between the carbon degradation and the amount of H-terminated edge sites among very different carbon materials thus far. Moreover, the linear relation in Fig. 7d suggests that the oxidation reactions detected in this work are not governed by diffusion (despite the large difference in nanoporosity among the samples), but chemical reactions. As the reaction time is the same for all samples (because the CV scan speed is the same), the amount of irreversible charge (Q_{ir}) can be regarded as a kind of reaction rate. Thus, Fig. 7d indicates that the reaction rate is proportional to the concentration of H-terminated edge sites. In other words, the reaction rate for the corrosion is the first order with respect to H-terminated edge sites.

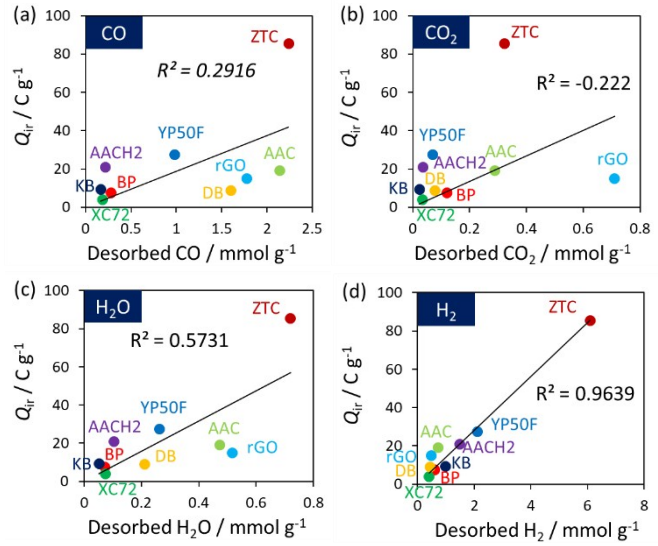

Fig. 7 The plot of Q_{ir} against the total amounts of (a) CO, (b) CO_2, (c) H_2O, and (d) H_2 evolutions. The calculation method of R^2 is shown in the Supplementary Information.

Although a good correlation can be found in Fig. 7d, some of the samples (AAC, rGO, and DB) show upward deviation from the approximate line, indicating the presence of corrosion sites other than H-terminated edge sites. Such sites may be specific types of oxygen-functional groups. To obtain a better correlation, the coefficient of determination (R^2) for the relation between Q_{ir} and the sum of the H-terminated edge sites (calculated by multiplying the entire H_2 evolution amount by 2) and the partial gas (CO, CO_2, or H_2O) evolution up to a certain temperature in each TPD experiment was plotted against the temperature in Fig. 8a. Interestingly, R^2 becomes very high (~0.99) when CO evolution amount is included at the range wider than 800 °C. This results implies that the CO-yielding functional groups are more likely to be responsible for the electrochemical degradations than CO_2- or H_2O-yielding functional groups. Fig. 8b shows the result of plotting Q_{ir} against the sum of the amount of H-terminated edge sites ($2 \times H_2$) and CO evolution. The R^2 reaches 0.9869, showing an excellent correlation between these two parameters. The obtained result suggests that the corrosion sites are not only H-terminated edge sites but also CO-yielding oxygen-functional groups, *i.e.*, hydroxyl groups, ethers and carbonyls.[37]

In order to confirm the above conclusions, the change of the TPD gas evolution in YP50F was examined before and after a single CV scan in the potential range of –0.5 to 1.0 V, and the result is shown in Table 2. As expected, H_2 and CO evolutions are decreased upon the CV scan, indicating the consumption of these edge sites by the electrochemical oxidation. The Q_{ir} of this CV cycle is 54.8 C g^{-1}, corresponding to 568 μmol g^{-1} of electrons. The decrease of H_2 evolution is 255 μmol g^{-1} (Table 2), corresponding to 510 μmol g^{-1} of H-terminated edge sites. Together with the decrease of CO evolution (84 μmol g^{-1}), it is estimated that 594 μmol g^{-1} of edge sites are reacted. This agrees very well with the value of the consumed electron (568 μmol g^{-1}), strongly supporting the aforementioned conclusions about the origin of the electrochemical oxidation. Also, the finding that the number of the reacted sites (594 μmol g^{-1}) revealed from Table 2 is very close to the number of

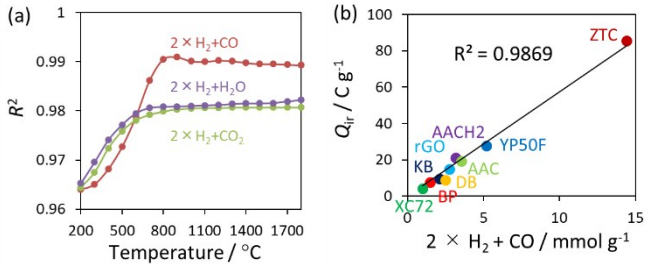

Fig. 8 (a) R^2 for the relation between Q_{ir} and the sum of the entire H-edge sites and the partial gas (CO, CO_2, and H_2O) evolution up to a certain temperature in the TPD experiment. (b) Q_{ir} versus the sum of the entire H-edge sites and the total CO evolution up to 1800 °C.

the consumed electron (568 μmol g^{-1}) suggests that the corrosion reaction is based on one-electron oxidation. It is also found that the ratio of the reacted sites are 17% for H-terminated edge sites and 11% for CO-yielding sites. Table 2 shows that the amount of CO_2-yielding oxygen functional groups remains almost the same before and after CV. Together with the fact that no new gas desorption peaks can be observed in the TPD run after CV, it is deduced that the oxidation products do not remain on the surface of carbon electrode, but may be resolved as gases during the CV measurement.

Table 2 The total gas evolutions during TPD measurement, before and after electrochemical oxidation of YP50F by a CV scan.

	H_2 (μmol g^{-1})	H_2O (μmol g^{-1})	CO (μmol g^{-1})	CO_2 (μmol g^{-1})
Before CV	1464	216	756	86
After CV	1209	247	672	92

Dependence on potential

While the above discussion is based on Q_{ir} at 1.0 V, the relation between Q_{ir} at different potentials and carbon edge sites is discussed here. Fig. 9a shows the R^2 values for the relations between $Q_{ir\text{-}xV}$ (x = 0.5 to 1.7) and TPD gas evolutions of H_2, CO, CO_2, H_2O, or H-terminated edge sites + CO. Since the measurement of ZTC was possible only up to 1.3 V because of its high reactivity, the data of ZTC is excluded in Fig. 9. While CO, CO_2, and H_2O show very low R^2 values which are mostly below 0, H_2 shows a good correlation with $Q_{ir\text{-}xV}$ in the potential range of 0.9 to 1.6 V. At the same potential range, the correlation of H + CO is further better, demonstrating that the electrochemical oxidation of H-terminated edge sites and CO-yielding sites occurs in this potential range (as Fig. 9b shows).

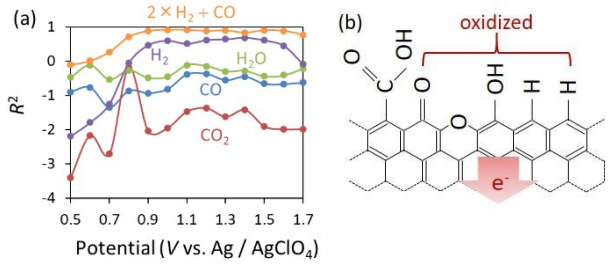

Fig. 9 (a) Correlation coefficient (R^2) of $Q_{ir\text{-}xV}$ against the amount of released gases at different potential range. (b) Illustration of electrochemical oxidation of carbon edge sites.

Dependence on electrolyte

In order to examine the effect of electrolyte on the carbon corrosion process, another organic electrolyte (1 M Et_4NBF_4 in acetonitrile) is used. This electrolyte is also used to commercial supercapacitors and is worth to be investigated. Fig. 10a shows the correlation between Q_{ir} and H_2 evolution for the carbon samples. Similarly to the case of Et_4NBF_4/PC (Fig. 7d), a good correlation can be found. When Q_{ir} is plotted against the sum of the entire H-edge sites and the total CO evolution up to 1800 °C, a better correlation is obtained (Fig. 10b), which accords to the result shown in Fig. 8b. This indicates that the edge-induced carbon corrosion is the main reason for positive electrode degradation also in the acetonitrile based organic electrolyte.

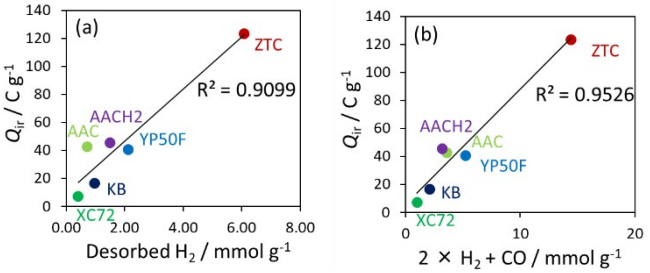

Fig. 10 (a) The plot of Q_{ir} against the amounts of H_2 evolution. (b) Q_{ir} versus the sum of the entire H-edge sites and the total CO evolution up to 1800 °C.

Conclusions

The origin of carbon degradation for early-stage electrochemical oxidation in organic electrolytes (1 M Et_4NBF_4/PC or 1 M Et_4NBF_4/acetonitrile) has been investigated. By correlating the degree of the electrochemical degradation with various carbon properties, we have found that the causal sites are H-terminated edge sites and oxygen-functional groups which are decomposed as CO in a TPD run, regardless of the types of carbon materials. Their crystallinity, porosity, and the number of radicals do not have any correlation with the carbon degradation in positive electrode. The observed good linear relationship between the degree of the electrochemical corrosion and the amount of such causal sites indicates that the reaction rate for the corrosion is the first order with respect to their amount. In addition, the detailed TPD analysis before and after the electrochemical oxidation through a CV scan reveals that the corrosion reaction is based on one-electron oxidation. Thus, we have demonstrated in this study that the quantitative analysis of carbon edge sites with the high-temperature TPD up to 1800 °C is an effective tool to judge the electrochemical stability of carbon materials and to understand the mechanism of the corrosion reaction for the first time. Moreover, this study presents the following guideline to achieve high voltage in supercapacitors: it is important to reduce the causal sites, for example, by fabricating carbon frameworks free from edge sites like single-walled carbon nanotubes and graphene mesosponge, or by chemical conversion of such sites into more stable forms.[38, 39]

Experimental

Carbon materials

Nine kinds of carbon materials were used in this work, including three kinds of activated carbons, four kinds of carbon blacks, rGO and ZTC[26] (Table 1). One of the activated carbons is anthracite-derived activated carbon (AAC) with an extremely high surface area (3650 m^2 g^{-1}).[30] Details of the sample preparation can be found in the Supplementary Information. The second activated carbon was prepared by H_2-treatment (850 °C for 1h) applied to AAC,[24] and it is referred to as AACH2. The third activated carbon is a coconut-shell-derived steam-activated carbon (YP50F; Kuraray Chemicals Co., Ltd)

View Article Online DOI: 10.1039/C8TA11005H

which is used indeed for commercial supercapacitors. The carbon blacks are BLACK PEALS 2000 (BP; Cabot Co., Ltd), VULCAN XC72 (XC72; Cabot Co., Ltd), Ketjen Black EC-300J (KB; Lion Specialty Chemicals., Ltd) and Denka Black (DB; Denka Co., Ltd). These carbon blacks are high-surface area types which are developed for catalyst supports or porous conductive additives. rGO has been known for its potential high surface area (2630 m^2 g^{-1}) and high performance as supercapacitor electrodes.[40] ZTC consists of ordered nanographene framework[34] and have ca. 10 times large amount of edge sites than activated carbons. Accordingly, it can be an extreme example of an edge-enriched carbon structure. ZTC was prepared by the method reported elsewhere.[26]

Characterization

Nitrogen adsorption isotherms of carbon materials were measured at –196 °C by using BELSORP-mini (MicrotracBEL Corp.). Specific surface area (S_{BET}) was calculated by using the Brunauer-Emmett-Teller (BET) method. Pore volume for pores less than 50 nm (V_{50nm}) was obtained from the N_2 adsorption amount at P/P_0 = 0.96, while total pore volume including a part of macropores (V_t) was obtained from the N_2 adsorption amount at P/P_0 = 0.99. Micropore volume (V_{micro}) was calculated by the Dubinin-Radushkevitch method. Mesopore volume (V_{meso}) was calculated by subtracting V_{micro} from V_{50nm}. Macropore volume (V_{macro}) was calculated by subtracting V_{50nm} from V_t. The carbon crystallinity was characterized by XRD (Shimadzu XRD-6100, X-ray source Cu Kα, 2θ range 2 ~ 50°, scan speed 0.625° min^{-1}) and also by Raman spectroscopy (JASCO NRS-3300FL, laser: 532.2 nm). The carbon edge sites were characterized by magnetic susceptibility measurement and high-sensitivity TPD.[29] Magnetic susceptibility was measured with a superconducting quantum interference device (SQUID). Curie constant (C) is calculated according to the Curie-Weiss law:

$$X_C = C/(T-\theta) \qquad (2)$$

where X_C is magnetic susceptibility, T is temperature, θ is the Curie temperature. The number of magnetic moment (N) is approximately calculated by the following equation:

$$C = \frac{Ng^2\mu_B^2 S(S+1)}{3k_B} \qquad (3)$$

where g is the Landé g-factor, μ_B is the Bohr magneton, S is the total spin quantum number, k_B is the Boltzmann constant. There are three possibilities of radical species at the carbon edge sites: π radicals (S = 1/2,)[28] σ radicals (S = 1/2), and triplet carbene (S = 1).[27] By dividing N with sample weight, spin density (N_{spin}) was obtained. The TPD measurement was performed on a sample (ca. 1 mg) by using a home-made high-vacuum apparatus allowing quantitative detection of gas evolutions such as H_2, H_2O, CO, and CO_2, during a heating of sample up to 1800 °C with a heating rate of 10 °C min^{-1}.[29]

Electrochemical measurement

Electrochemical measurement was performed in a three-electrode cell at 25 °C. For activated carbons and ZTC, a carbon sample was mixed with binder polymer (PTFE; PTFE 6–J, Du Pont–Mitsui Fluorochemicals Co. Ltd.) and carbon black (Denka black, Denki Kagaku Kogyo Kabushiki Kaisha) by the ratio of 90:5:5. For carbon blacks and rGO, a sample was mixed with PTFE by the ratio of 85:15 without additional carbon black, because these samples have enough high electric conductivity and it was difficult to form a uniform electrode sheet with a small amount of PTFE. The resulting mixture was moulded into a square sheet (1×1 cm^2, 5–10 mg), and sandwiched with a Pt mesh, to be a working electrode. An electrolyte is 1 M Et_4NBF_4 in propylene carbonate (PC) or acetonitrile. An activated carbon fibre (Unitika, A20) was used for a counter electrode, which was prepared by the same manner for activated carbon electrodes except its loading amount (ca. 20 mg). A reference electrode was $Ag/AgClO_4$. With the three-electrode cell, cyclic voltammetry (CV) was performed by the following manner. First, CV scan (1 mV s^{-1}) was repeated four times in the potential range of –0.5 to 0.5 V, and then the upper potential limit was gradually expanded by 0.1 V up to 2.1 V. At each potential range, CV scan was repeated four times. The degradation of the carbon electrode was judged by irreversible charge (Q_{ir} [C]), calculated according to the following equation:

$$Q_{\mathrm{ir}} = Q_{\mathrm{positive}} - Q_{\mathrm{negative}} \qquad (4)$$

where Qpositive and Qnegative are total charges during the first positive-direction scan and during the first negative-direction scan, respectively. $Q_{positive}$ and $Q_{negative}$ were obtained by integrating CV current with time[20, 41] in the potential range between the open circuit potential (–0.2 to 0 V) to the maximum potential at a CV scan (x [V]; $0.5 \le x \le 1.9$).

Conflicts of interest

There are no conflicts to declare.

Acknowledgements

The authors appreciate Prof. H. Shiku for his kind advice on electrochemical characterization of carbon corrosion reactions. The authors are thankful to Ms. Qiong Lin and Ms. Mao Ohwada for their experimental contributions. This work was supported by JSPS KAKENHI (grant Nos. 15H01999 and 17H01042); the Dynamic Alliance for Open Innovation Bridging Human, Environment, and Materials program; and the Network Joint Research Centre for Materials and Devices. R. T. acknowledges the China Scholarship Council for the financial support. MINECO and FEDER (CTQ2015-66080-R MINECO/FEDER) are acknowledged for financial support.

References

1 M. Sevilla, W. Gu, C. Falco, M. M. Titirici, A. B. Fuertes and G. Yushin, *J. Power Sources*, 2014, **267**, 26-32.
2 T. Y. Yang, R. F. Zhou, D. W. Wang, S. P. Jiang, Y. Yamauchi, S. Z. Qiao, M. J. Monteiro and J. Liu, *Chem. Commun.*, 2015, **51**, 2518-2521.
3 R. Berenguer, F. J. Garcia-Mateos, R. Ruiz-Rosas, D. Cazorla-Amoros, E. Morallon, J. Rodriguez-Mirasol and T. Cordero, *Green Chemistry*, 2016, **18**, 1506-1515.
4 K. V. Kumar, S. Gadipelli, K. Preuss, H. Porwal, T. T. Zhao, Z. X. Guo and M. M. Titirici, *Chemsuschem*, 2017, **10**, 199-209.
5 F. J. Martin-Jimeno, F. Suarez-Garcia, J. I. Paredes, M. Enterria, M. F. R. Pereira, J. I. Martins, J. L. Figueiredo, A. Martinez-Alonso and J. M. D. Tascon, *Acs Applied Materials & Interfaces*, 2017, **9**, 44740-44755.

6 J. M. Munuera, J. I. Paredes, M. Enterria, A. Pagan, S. Villar-Rodil, M. F. R. Pereira, J. I. Martins, J. L. Figueiredo, J. L. Cenis, A. Martinez-Alonso and J. M. D. Tascon, *Acs Applied Materials & Interfaces*, 2017, **9**, 24085-24099.
7 X. T. Xu, J. Tang, H. Y. Qian, S. J. Hou, Y. Bando, M. S. A. Hossain, L. K. Pan and Y. Yamauchi, *Acs Applied Materials & Interfaces*, 2017, **9**, 38737-38744.
8 S. L. Zhai, H. E. Karahan, L. Wei, X. C. Chen, Z. Zhou, X. Wang and Y. Chen, *Energy Storage Materials*, 2017, **9**, 221-228.
9 P. Mei, Y. V. Kaneti, M. Pramanik, T. Takei, O. Dag, Y. Sugahara and Y. Yamauchi, *Nano Energy*, 2018, **52**, 336-344.
10 S. L. Zhai, C. J. Wang, H. E. Karahan, Y. Q. Wang, X. C. Chen, X. Sui, Q. W. Huang, X. Z. Liao, X. Wang and Y. Chen, *Small*, 2018, **14**.
11 S. L. Zhai, L. Wei, H. E. Karahan, Y. Q. Wang, C. J. Wang, A. Montoya, Q. Shao, X. Wang and Y. Chen, *Carbon*, 2018, **132**, 698-708.
12 P. Azaïs, L. Duclaux, P. Florian, D. Massiot, M.-A. Lillo-Rodenas, A. Linares-Solano, J.-P. Peres, C. Jehoulet and F. Béguin, *J. Power Sources*, 2007, **171**, 1046-1053.
13 P. W. Ruch, D. Cericola, A. Foelske-Schmitz, R. Kötz and A. Wokaun, *Electrochim. Acta*, 2010, **55**, 4412-4420.
14 P. W. Ruch, D. Cericola, A. Foelske, R. Kötz and A. Wokaun, *Electrochim. Acta*, 2010, **55**, 2352-2357.
15 M. Tokita, N. Yoshimoto, K. Fujii and M. Morita, *Electrochim. Acta*, 2016, **209**, 210-218.
16 O. Bohlen, J. Kowal and D. U. Sauer, *J. Power Sources*, 2007, **172**, 468-475.
17 M. Hahn, A. Würsig, R. Gallay, P. Novák and R. Kötz, *Electrochem. Commun.*, 2005, **7**, 925-930.
18 R. Kötz, M. Hahn, P. Ruch and R. Gallay, *Electrochem. Commun.*, 2008, **10**, 359-362.
19 M. Hahn, R. Kötz, R. Gallay and A. Siggel, *Electrochim. Acta*, 2006, **52**, 1709-1712.
20 D. Weingarth, H. Noh, A. Foelske-Schmitz, A. Wokaun and R. Kötz, *Electrochim. Acta*, 2013, **103**, 119-124.
21 A. Izadi-Najafabadi, S. Yasuda, K. Kobashi, T. Yamada, D. N. Futaba, H. Hatori, M. Yumura, S. Iijima and K. Hata, *Adv. Mater.*, 2010, **22**, E235-+.
22 H. Nishihara, T. Simura, S. Kobayashi, K. Nomura, R. Berenguer, M. Ito, M. Uchimura, H. Iden, K. Arihara, A. Ohma, Y. Hayasaka and T. Kyotani, *Adv. Funct. Mater.*, 2016, **26**, 6418-6427.
23 S. Ishimoto, Y. Asakawa, M. Shinya and K. Naoi, *J. Electrochem. Soc.*, 2009, **156**, A563.
24 D. Cazorla-Amorós, D. Lozano-Castelló, E. Morallón, M. J. Bleda-Martínez, A. Linares-Solano and S. Shiraishi, *Carbon*, 2010, **48**, 1451-1456.
25 C. H. Yang, Q. D. Nguyen, T. H. Chen, A. S. Helal, J. Li and J. K. Chang, *Acs Sustainable Chemistry & Engineering*, 2018, **6**, 1208-1214.
26 K. Nueangnoraj, H. Nishihara, T. Ishii, N. Yamamoto, H. Itoi, R. Berenguer, R. Ruiz-Rosas, D. Cazorla-Amorós, E. Morallón, M. Ito and T. Kyotani, *Energy Storage Materials*, 2015, **1**, 35-41.
27 L. R. Radovic and B. Bockrath, *J. Am. Chem. Soc.*, 2005, **127**, 5917-5927.
28 S. Fujii and T. Enoki, *Acc. Chem. Res.*, 2013, **46**, 2202-2210.
29 T. Ishii, S. Kashihara, Y. Hoshikawa, J.-i. Ozaki, N. Kannari, K. Takai, T. Enoki and T. Kyotani, *Carbon*, 2014, **80**, 135-145.
30 D. Lozano-Castello, M. A. Lillo-Rodenas, D. Cazorla-Amoros and A. Linares-Solano, *Carbon*, 2001, **39**, 741-749.
31 M. Thommes, K. Kaneko, A. V. Neimark, J. P. Olivier, F. Rodriguez-Reinoso, J. Rouquerol and K. S. W. Sing, *Pure Appl. Chem.*, 2015, **87**, 1051-1069.
32 K. Xu, M. S. Ding and T. R. Jow, *Electrochim. Acta*, 2001, **46**, 1823-1827.
33 T. X. Nguyen, N. Cohaut, J. S. Bae and S. K. Bhatia, *Langmuir*, 2008, **24**, 7912-7922.
34 H. Nishihara, H. Fujimoto, H. Itoi, K. Nomura, H. Tanaka, M. T. Miyahara, P. A. Bonnaud, R. Miura, A. Suzuki, N. Miyamoto, N. Hatakeyama, A. Miyamoto, K. Ikeda, T. Otomo and T. Kyotani, *Carbon*, 2018, **129**, 854-862.
35 J. Maruyama, T. Shinagawa, A. Hayashida, Y. Matsuo, H. Nishihara and T. Kyotani, *Chemelectrochem*, 2016, **3**, 650-657.
36 U. Zielke, K. J. Huttinger and W. P. Hoffman, *Carbon*, 1996, **34**, 999-1005.
37 J. L. Figueiredo, M. F. R. Pereira, M. M. A. Freitas and J. J. M. Orfao, *Carbon*, 1999, **37**, 1379-1389.
38 R. Berenguer, R. Ruiz-Rosas, A. Gallardo, D. Cazorla-Amoros, E. Morallon, H. Nishihara, T. Kyotani, J. Rodriguez-Mirasol and T. Cordero, *Carbon*, 2015, **95**, 681-689.
39 F. J. Garcia-Mateos, R. Berenguer, M. J. Valero-Romero, J. Rodriguez-Mirasol and T. Cordero, *Journal of Materials Chemistry A*, 2018, **6**, 1219-1233.
40 D. F. Sun, X. B. Yan, J. W. Lang and Q. J. Xue, *J. Power Sources*, 2013, **222**, 52-58.
41 K. Xu, S. P. Ding and T. R. Jow, *J. Electrochem. Soc.*, 1999, **146**, 4172-4178.

View Article Online
DOI: 10.1039/C8TA11005K

Table of Contents Entry

Insight into the origin of carbon corrosion in positive electrodes of supercapacitors

Rui Tang, Kaishi Taguchi, Hirotomo Nishihara*, Takafumi Ishii, Emilia Morallón, Diego Cazorla-Amorós, Toshihiro Asada, Naoya Kobayashi, Yasuji Muramatsu and Takashi Kyotani

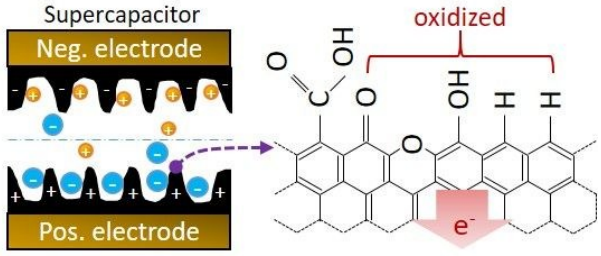

The carbon corrosion sites at positive-electrodes of supercapacitors are identified as <u>H-terminated edge sites, ether, hydroxyl and carbonyl groups</u>.